Supporting Information

Towards absolute molecular numbers in DNA-PAINT

Johannes Stein[†,‡], Florian Stehr[†,‡], Patrick Schueler[†], Philipp Blumhardt[†], Florian Schueder[†,§], Jonas Mücksch[†], Ralf Jungmann[†,§] and Petra Schwille[†,*]

[†]Max Planck Institute of Biochemistry, 82152 Martinsried near Munich, Germany.
[§]Faculty of Physics, Ludwig Maximilian University, 80539 Munich, Germany.

Supplementary methods

Materials

Unmodified, dye-labeled, and biotinylated DNA oligonucleotides were purchased from MWG Eurofins. DNA scaffold strands were purchased from Tilibit (p7249, identical to M13mp18). Streptavidin was purchased from Thermo Fisher (cat: S-888). BSA-Biotin was obtained from Sigma-Aldrich (cat: A8549). Glass slides were ordered from Thermo Fisher (cat: 10756991) and coverslips were purchased from Marienfeld (cat: 0107032). Freeze 'N Squeeze columns were ordered from Bio-Rad (cat: 732-6165). Tris 1M pH 8.0 (cat: AM9856), EDTA 0.5M pH 8.0 (cat: AM9261), Magnesium 1M (cat: AM9530G) and Sodium Chloride 5M (cat: AM9759) were ordered from Ambion. Ultrapure water (cat: 10977-035) was purchased from Thermo Fisher Scientific. Tween-20 (cat: P9416-50ML), Glycerol (cat. 65516-500ml) and (+-)-6-Hydroxy-2,5,7,8-tetra-methylchromane-2-carboxylic acid (Trolox) (cat: 238813-5G) were purchased from Sigma-Aldrich. Two-component epoxy glue (cat: 886519 - 62) was purchased from Conrad Electronic SE.

Buffers

Four buffers were used for sample preparation and imaging: Buffer A+ (10 mM Tris-HCl pH 7.5, 100 mM NaCl, 0.05% Tween 20, pH 7.5); Buffer B+ (5 mM Tris-HCl pH 8.0, 10 mM MgCl2, 1 mM EDTA, 0.05% Tween 20, pH 8); Enzyme buffer for POC oxygen scavenging system (10 mM Tris pH 7.5, 50 mM KCl, 20% glycerol); 10x folding buffer (100 mM Tris,10 mM EDTA pH 8.0, 125 mM MgCl2).

DNA origami design, assembly and purification

DNA origami structures were designed using the design module of Picasso[1] (see **Figure 4**, top for docking strand positions). Folding of structures was performed using the following components: single-stranded DNA scaffold (0.01 µM), core staples (0.5 µM), biotin staples (0.5 µM), modified staples (each 0.5 µM), 1× folding buffer in a total of 50 µl for each sample. Annealing was done by cooling the mixture from 80 to 25 °C in 3 h in a thermocycler. Structures were purified using gel electrophoresis (3 h at 60 V). For detailed instructions see[1,2].

DNA origami sample preparation

DNA origami samples were prepared as described before[1]. A glass slide was glued onto a coverslip with the help of double-sided tape (Scotch, cat. no. 665D) to form a flow chamber with inner volume of ~20 µl. First, 20 µl of biotin-labeled bovine albumin (1 mg/ml, dissolved in buffer A+) was flushed into the chamber and incubated for 3 min. The chamber was then washed with 40 µl of buffer A+. 20 µl of streptavidin (0.5 mg/ml, dissolved in buffer A+) was then flushed through the chamber and incubated for 3 min. After washing with 40 µl of buffer A+ and subsequently with 40 µl of buffer B+, 20 µl of biotin-labeled DNA structures (dilution from DNA origami stock dependent on origami yield after gel purification. Adjusted for each origami species individually to obtain sparse DNA origami surface density. Starting dilution ~1:4) were flushed into the chamber and incubated for 10 min. The chamber was washed with 40 µl of buffer B+. Finally, 40 µl of the imager solution was flushed into the chamber, which was subsequently sealed with two-component epoxy glue before imaging. Adjustment of imager concentrations: The imager concentrations used for all experiments were c = 5, 10 and 20 nM. As described in **Supplementary Figure 6**, we first prepared a larger volume of 20 nM imager solution, from which in two subsequent 1:1 dilution steps the 10 nM and 5 nM solutions were prepared. Sequence design of imager and docking strands can be found in **Supplementary Table 2**.

Super-resolution microscopy setup

Fluorescence imaging was carried out on an inverted custom-built microscope[3] (see setup sketch in **Supplementary Figure 2**a) in an objective-type TIRF configuration with an oil-immersion objective (Olympus UAPON, 100×, NA 1.49). One laser was used for excitation: 561 nm (1 W, DPSS-system, MPB). Laser power

was adjusted by polarization rotation with a half-wave plate (Thorlabs, WPH05M-561) before passing a polarizing beam-splitter cube (Thorlabs, PBS101). To spatially clean the beam-profile the laser light was coupled into a single-mode polarization-maintaining fiber (Thorlabs, P3-488PM-FC-2) using an aspheric lens (Thorlabs, C610TME-A). The coupling polarization into the fiber was adjusted using a zero-order half wave plate (Thorlabs, WPH05M-561). The laser light was re-collimated after the fiber using an achromatic doublet lens (Thorlabs, AC254-050-A-ML) resulting in a collimated FWHM beam diameter of ~6 mm. The Gaussian laser beam profile was transformed into a collimated flat-top profile using a refractive beam shaping device (AdlOptica, piShaper 6_6_VIS). The laser beam diameter was magnified by a factor of 2.5 using a custom-built telescope (Thorlabs, AC254-030-A-ML and Thorlabs, AC508-075-A-ML). The laser light was coupled into the microscope objective using an achromatic doublet lens (Thorlabs, AC508-180-A-ML) and a dichroic beam splitter (AHF, F68-785). Fluorescence light was spectrally filtered with a laser notch filter (AHF, F40-072) and a bandpass filter (AHF Analysentechnik, 605/64) and imaged on a sCMOS camera (Andor, Zyla 4.2) without further magnification (Thorlabs, TTL180-A) resulting in an effective pixel size of 130 nm (after 2 × 2 binning). Microscopy samples were mounted into a closed water-based temperature chamber (Okolab, H101-CRYO-BL) on a x-y-z stage (ASI, S31121010FT and ASI, FTP2050) that was used for focusing with the microscope objective being at fixed position. The temperature of the objective was actively controlled using the same water cycle as the temperature chamber. Focus stabilization was achieved via the CRISP autofocus system (ASI @ 850 nm) in a feedback loop with a piezo actuator (Piezoconcept, Z-INSERT100) moving the sample. The CRISP was coupled into the excitation path of the microscope using a long pass dichroic mirror (Thorlabs, DMLP650L). Our custom TIRF setup was used for all Figures.

Imaging conditions

All fluorescence microscopy data was recorded with our sCMOS camera (2048 × 2048 pixels, pixel size: 6.5 µm). The camera was operated with the open source acquisition software µManager[4] at 2x2 binning and cropped to the center 700 × 700 pixel FOV. The exposure time was set to 200 ms, the read out rate to 200 MHz and the dynamic range to 16 bit. For lbFCS measurements the laser power was set to 1.4 mW (see **Supplementary Figure 2**), corresponding to an average intensity of ~10 W/cm^2 over the circular illuminated area of 130 μm in diameter. The acquisition lengths for lbFCS measurements were set to: 9,000 frames (c = 20 & 10 nM) and 18,000 frames (c = 5 nM). Longer acquisition lengths at lower imager concentrations ensure that sufficient imager binding events are registered from each DS cluster as a prerequisite for robust autocorrelation analysis[5]. For high resolution imaging the laser power was set to 70 mW (intensity of ~500 W/cm^2) and the acquisition length to 5,000 frames.

Super-resolution reconstruction & data analysis

Refer to **Supplementary Figure 1** for a detailed step-by-step guide through all processing steps after data acquisition. The lbFCS software package and installation instructions are available at https://github.com/schwille-paint/lbFCS. A full integration in the Picasso[1] software package is currently under construction.

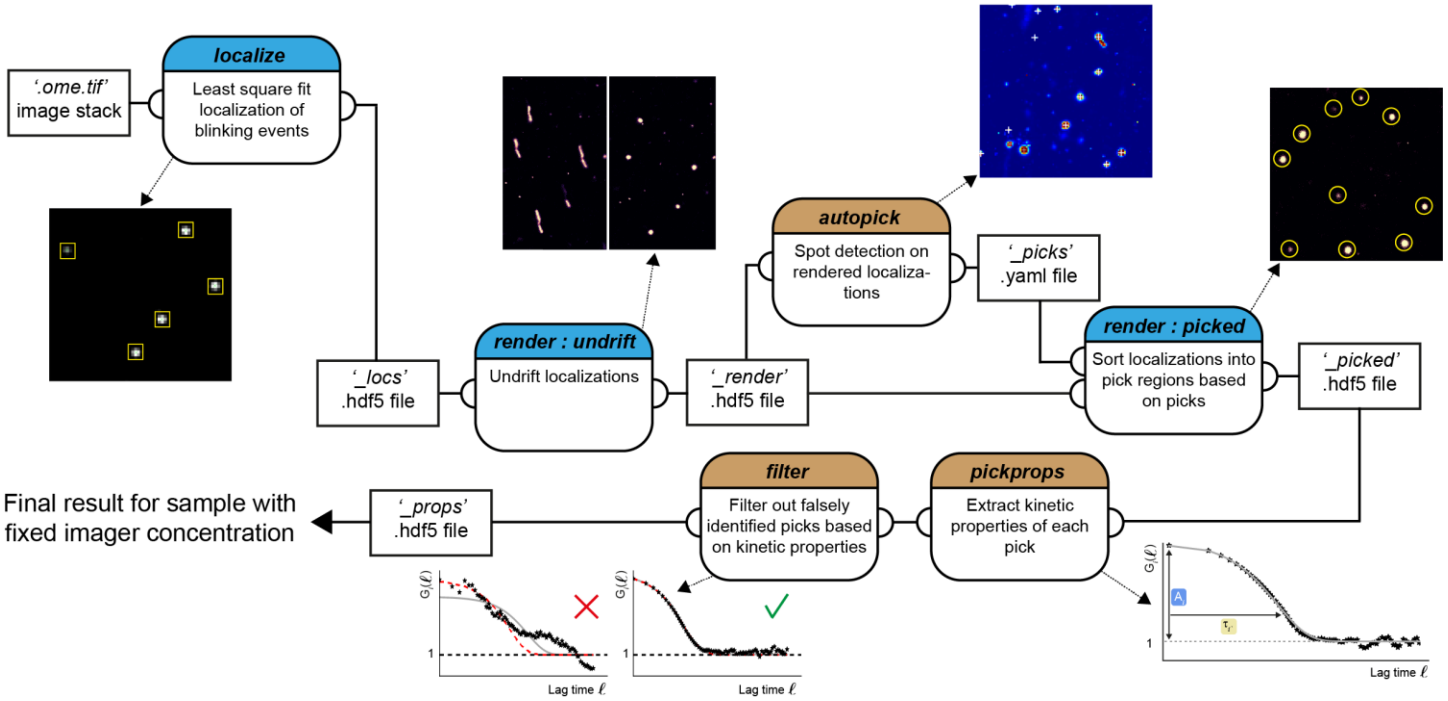

Supplementary Figure 1. Step-by-step guide through lbFCS analysis. (a) Software flow diagram depicting how final autocorrelation analysis result is obtained from DNA-PAINT raw-data. Rectangles represent saved data containing custom file extension and data format. Rounded boxes represent modules from 'picasso' python package[1] (blue) (https://github.com/jungmannlab/picasso) or custom python modules (ocher) (see **Supplementary Materials**) with half open circles indicating either input or output files according to flow direction. All additional input parameters of the modules used are listed in **Supplementary Table 3**. For a detailed description on the 'filter' module see **Supplementary Figure 3**.

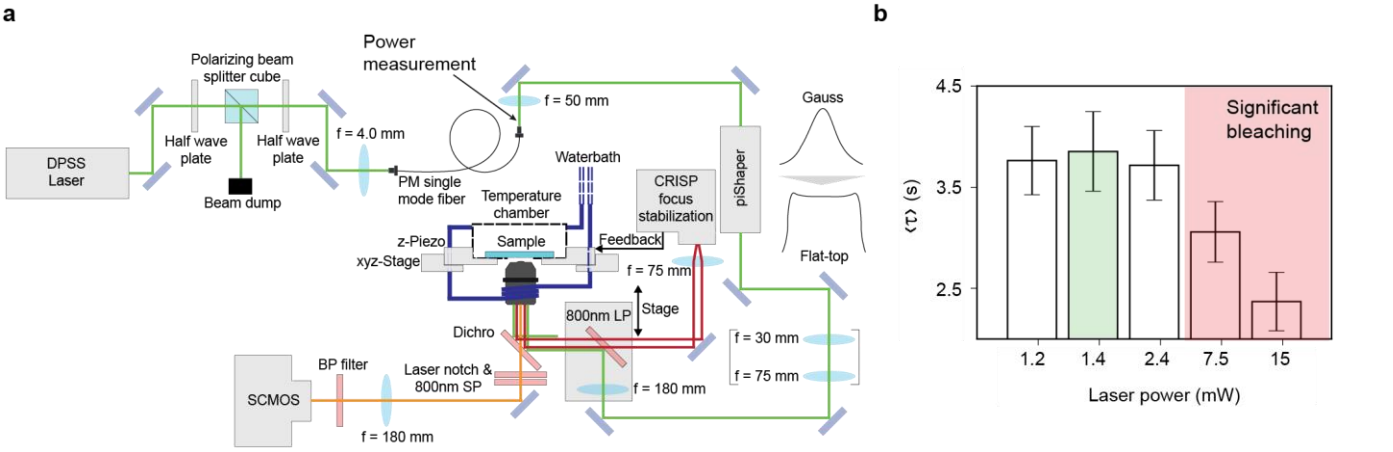

Supplementary Figure 2. Custom-built TIRF microscope and laser power series. (a) Sketch of custom-built TIRF microscope. See Supplementary Methods for details on components. (b). Power series on sample containing single docking strand DNA origami at 21°C (the temperature condition yielding the longest imager residence times, i.e. lowest k_{off}). The laser power was measured after the fiber exit (see (a)). The red area highlights the regime where the laser power is high enough to photobleach the dye molecules of bound imager strands before dissociation which therefore significantly affects the extracted values of $\langle\tau\rangle$. We chose a laser power at ~1.4 mW (green), where we did not affect the extracted rates but were still able to robustly detect fluorescence bursts for super-resolution reconstruction.

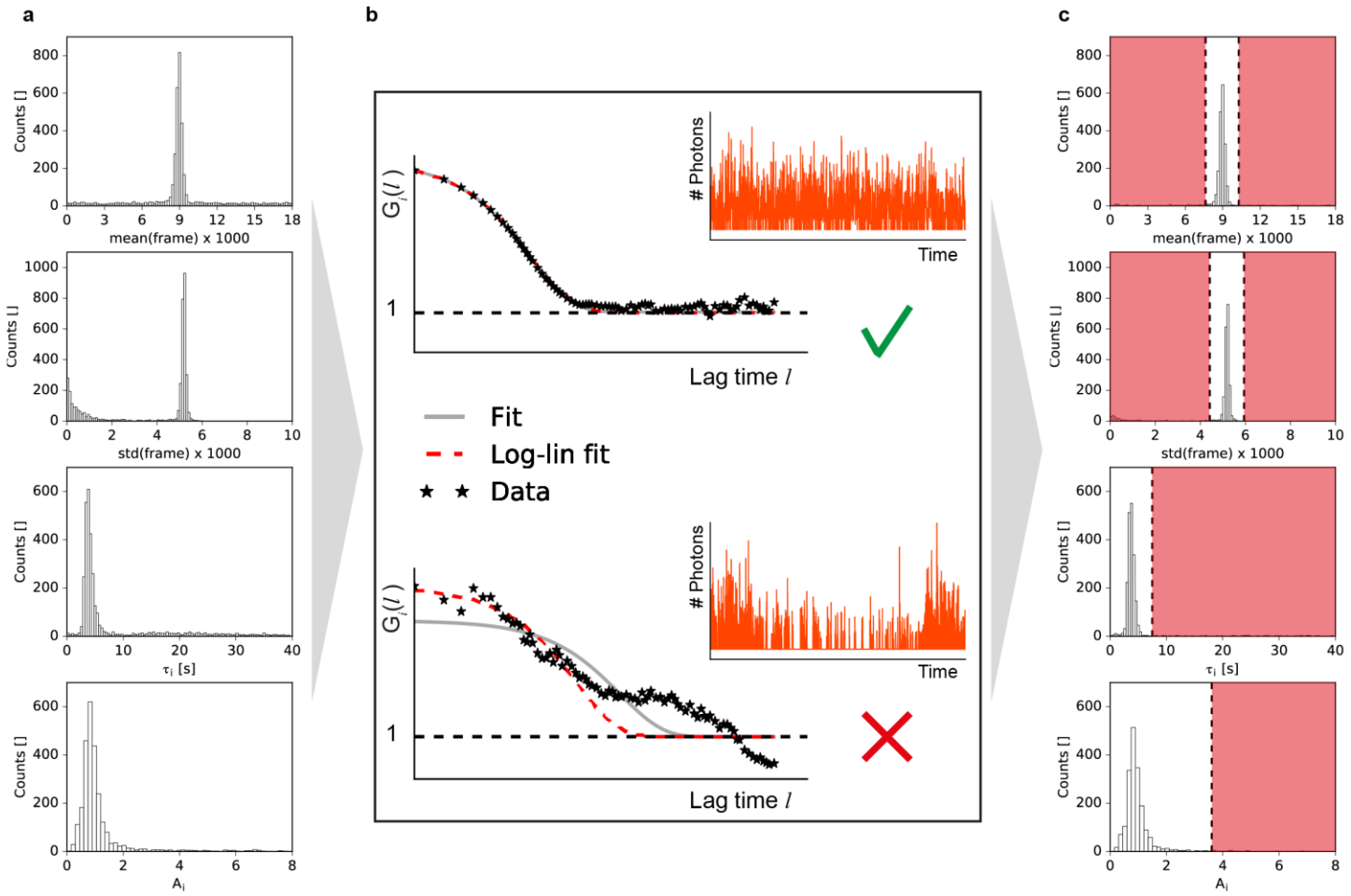

Supplementary Figure 3. Filtering out clusters whose intensity vs. time traces exhibit flawed dynamics. (a) Final distributions of kinetic variables as obtained before 'filter' module (see **Supplementary Figure 1**) over all picks of a sample containing DNA origami with 12 DSs at *c* = 5 nM. The variable mean(frame) and std(frame) refer to the mean (standard deviation) of the timestamp (frame) of all localizations in a pick. (b) The 'pickprops' module (see **Supplementary Figure 1**) applies two fitting procedures to the autocorrelated intensity vs. time trace (black stars): (1) a non-linear least square fit according to the equation $\mathrm{G}_i(l) = \mathrm{A}_i e^{l/\tau_i} + 1$ (gray) and, (2) a linear fit to the logarithmized autocorrelation function using the logarithmic form of the same equation $\log(\mathrm{G}_i(l) - 1) = \mathrm{A}_i + l/\tau_i$ (red dashed). The linearized logarithmic fit does only take into account the first 10 data points of the autocorrelation. In the first filtering step the two different τ_i for each pick obtained by the two fitting approaches are compared. If the value τ_i as resulting by (2) deviates more than 20 % of the value τ_i as resulting by (1) the pick is disregarded for further analysis. The resulting distributions over all picks after this filtering step are shown in (c). In the second filtering step the median over all picks for each of the variables mean(frame), std(frame), τ_i and A_i is calculated. Picks with the following attributes are disregarded for further analysis (indicated by the red area): mean(frame) < 0.85 x median or > 1.15 x median, std(frame) < 0.85 median, τ_i > 2 x median, A_i > 4 x median.

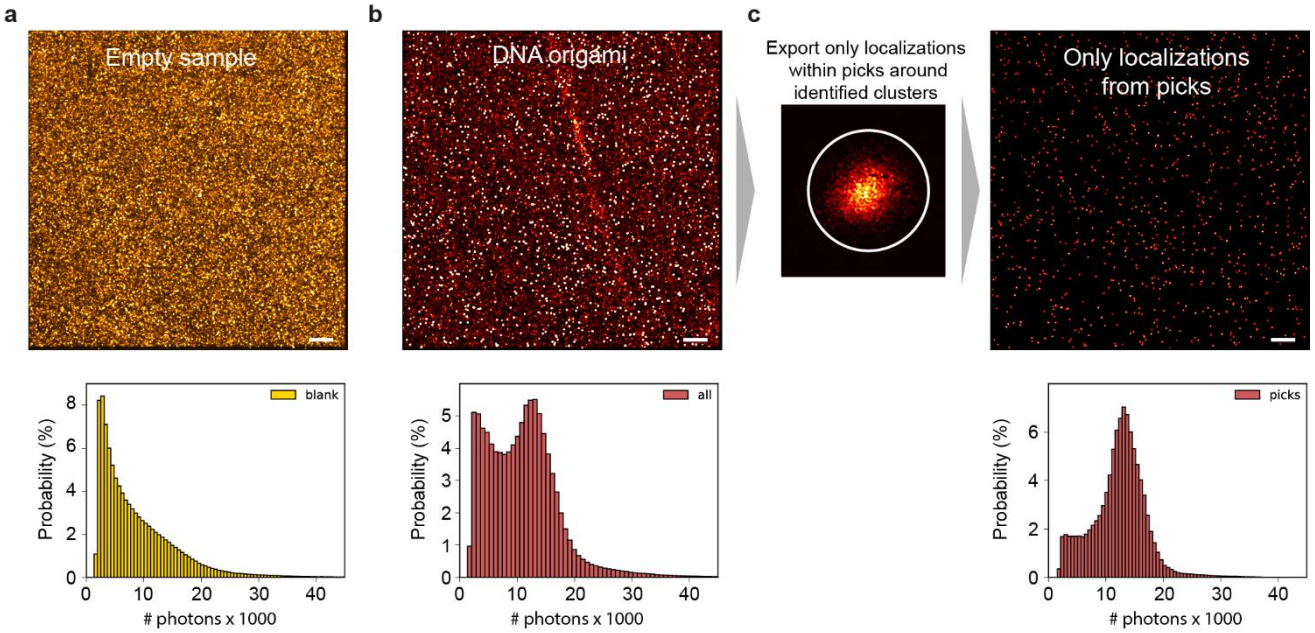

Supplementary Figure 4. Unspecific surface binding interactions. (a) DNA-PAINT image of a surface-passivated sample (BSA-Biotin-Streptavidin, see sample preparation in **Supplementary Methods**) containing no DNA origami but only 10 nM imager in the solution. Unspecific binding of imager to the surface is registered as blinking events leading to a homogeneous distribution of localizations over the surface. The histogram below shows the number of photons counted in each localization event. (b) DNA-PAINT image of sample containing DNA origami acquired under the same conditions as (a). DNA origami appear as bright spots whereas unspecific binding still leads to a homogeneous surface coverage of localizations. The photon count histogram now displays a distinct peak around 13,000 originating from specific binding interactions to DNA origami in addition to the same unspecific distribution as in (a). (c) For further lbFCS analysis we only process localizations within identified localization clusters (picks, white circle, see also **Figure 1**b). The photon count histogram of the localizations from all picks exhibits the same peak as in (b) from specific binding interactions but localizations originating from unspecific binding are minimized. Scale bars, 5 μm.

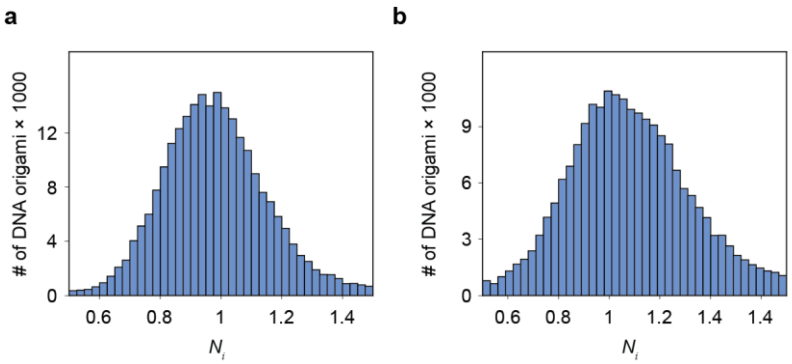

Supplementary Figure 5. 1DS counting results for lbFCS at varying temperature and MgC_2 concentration. (a) Sum of the counting results for lbFCS measurements at 21 - 24 °C (see **Figure 3**a). (b) Sum of the counting results for lbFCS measurements at 5-15 mM $MgCl_2$ (see **Figure 3**b).

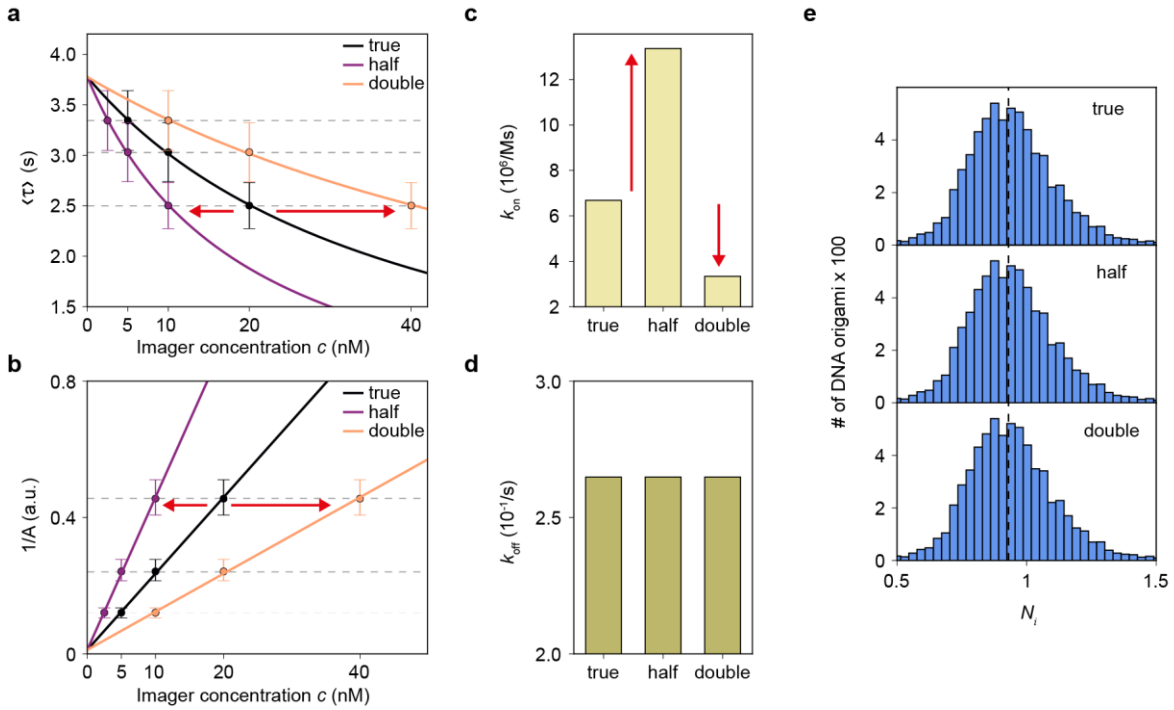

Supplementary Figure 6. Self-calibrating counting independent of absolute imager concentration. (a) As described in the **Supplementary Methods** (sample preparation) we adjusted the imager concentrations to *c* = 5, 10 and 20 nM starting with the highest concentration *c* = 20 nM which we subsequently diluted twice at a ratio 1:1. Here, we illustrate that the counting ability of lbFCS does in fact not depend on the absolute imager concentration. The black ⟨τ⟩ vs. *c* fit shows the results of the lbFCS measurement series on samples containing 1DS origami structures (referred to as "true" due to *c* = 5, 10 and 20 nM). Next, we assume that we actually failed to adjust the first dilution by a factor of 2 to 40 nM instead of 20 nM resulting in a horizontal shift of the three measurement points to the right (red arrow). The orange ⟨τ⟩ vs. *c* curve hence fits the data points at *c* = 10, 20 and 40 nM ("double"). Similarly, we go through the "half" scenario where we started with 10 nM and ended up with 5 and 2.5 nM shifting the data points horizontally to the left (red arrow, purple fit). (b) Same as (a) but for 1/A obtained from the three data sets. As described in the main text, all three fits cross pass through the origin since the concentration ratios are still conserved. (c) k_{on} obtained from the three ⟨τ⟩ vs. *c* fits in (a). The relative offset in the imager concentration *c* inversely translates into an offset in k_{on} (i.e. k_{on} doubles for "half" and halves for "double". See **eq. 2**) (d) k_{off} obtained from the three ⟨τ⟩ vs. *c* fits in (a). k_{off} is unaffected by the introduced offset in *c* (also visible at the identical y-axis intersections in (a). Compare **eq. 2** for *c*→0). (e) lbFCS yields identical counting results (sum N_i over the three measurements displayed) independent of the introduced offset in *c* as it cancels out when multiplied by k_{on}: $N_i = \frac{1}{A_i}\frac{k_{off}}{k_{on}c}$.

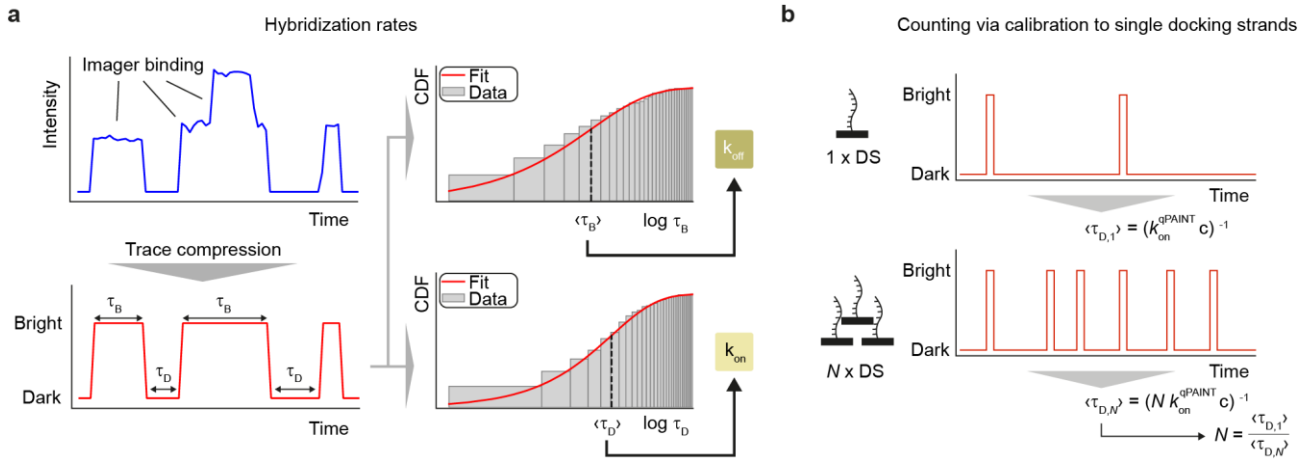

Supplementary Figure 7. The qPAINT approach. (a) Current standard for extracting imager hybridization kinetics from DNA-PAINT data. The intensity vs. time trace (blue) is compressed into a system of two states (red): i) Bright (bound imager) and ii) Dark (no imager). Here, information regarding simultaneous binding of multiple imagers resulting in higher intensity values is lost. All dwell times in both states, referred to as bright times τ_B and dark times τ_D, are extracted from the compressed trace and processed into cumulative histograms. Short disruptions of fluorescence bursts in the intensity trace (i.e. between two bright times) less than a predefined 'ignore' parameter are discarded (i.e. the two bright times a treated as one bright time with the combined duration. Standard: ignore = 1 frame). The histograms are fitted with the fit model[1] $F(\tau_m) = \left(1 - \exp\left(\frac{\tau_m}{\langle\tau_m\rangle}\right)\right) a + b$, where $m = \mathrm{B}, \mathrm{D}$ and the angle brackets denote the mean of the respective distribution. a and b are empirical fit parameters introduced for improved qPAINT counting performance (see implementation at https://github.com/jungmannlab/picasso[1]). In order to apply this fit model with three parameters to an intensity vs. time trace from a localization cluster, the trace needs to exhibit at least three unique dark times (e.g. two dark times of lengths = 2 frames, three dark time of lengths = 5 frames and one dark time of length 11 frames. See **Supplementary Figure 9**). The imager hybridization rates can be obtained via the following relations[1,6,7]: $k_{off} = \langle\tau_\mathrm{B}\rangle^{-1}$ and $k_{on}c = \langle\tau_\mathrm{D}\rangle^{-1}$. (b) Counting with qPAINT relies on calibration to the imager influx rate during a DNA-PAINT measurement obtained from single docking strands (1DS). The influx rate is defined as the inverse mean dark time obtained from a 1DS fluorescence vs. intensity trace $\langle\tau_{\mathrm{D},1}\rangle^{-1} = k_{on}^{qPAINT} c$. qPAINT is based on the assumption that a cluster of *N* DS will produce an intensity vs. time trace with a mean dark time $\langle\tau_{\mathrm{D},N}\rangle$ shortened by a factor of *N* compared to a 1DS. Hence, qPAINT counting results for each localization cluster *i* are obtained via the relation: $N_i = (k_{on}^{qPAINT} c \times \langle\tau_{\mathrm{D},i}\rangle)^{-1} = \langle\tau_{\mathrm{D},1}\rangle / \langle\tau_{\mathrm{D},i}\rangle$.

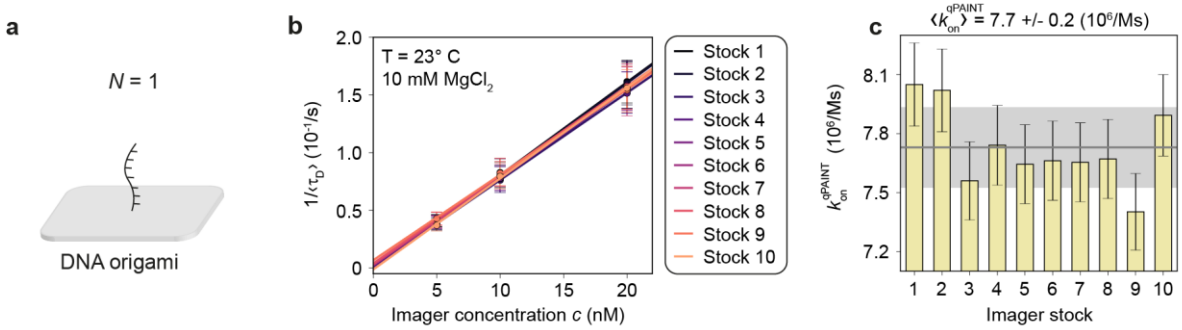

Supplementary Figure 8. qPAINT calibration from single docking strands. (a) For qPAINT calibration we used the measurements obtained on 1DS structures as in **Figure 2**a-e. (b) $1/\langle\tau_D\rangle$ vs. *c* fit for the 10 concentration series. As defined in **Supplementary Figure 7**, $1/\langle\tau_D\rangle = k_{on}^{qPAINT} c$ which means that k_{on}^{qPAINT} required for qPAINT calibration can directly be read off the slope of the fit. (c) Scatter in k_{on}^{qPAINT} obtained from fits in (b). Mean and standard deviation are indicated as grey line and light grey area, respectively. The mean of $\langle k_{on}^{qPAINT}\rangle$ = (7.7 ± 0.2 × 10^6) $M^{-1}s^{-1}$ was used as calibration for all qPAINT counting results. We would like to note that the high precision in k_{on}^{qPAINT} is due to profiting from the filtering procedure introduced in **Supplementary Figure 3**, which in turn is based on the unique property of the autocorrelation analysis of lbFCS to identify and exclude docking strands exhibiting flawed dynamics.

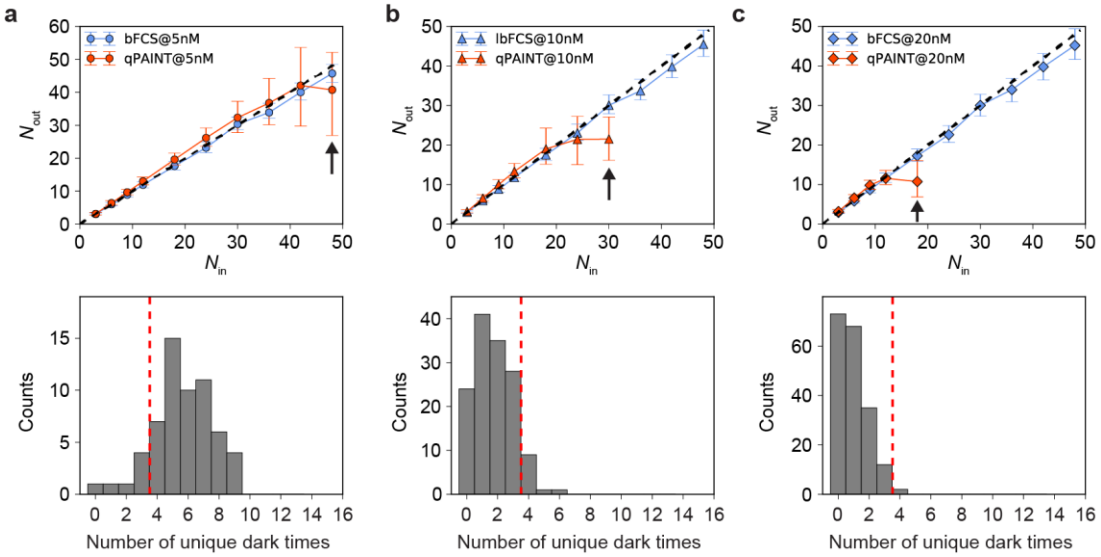

Supplementary Figure 9. N_{out} vs. N_{in} at varying imager concentrations. (a) Top: median of the counting results N_{out} vs. N_{in} plot comparing the results obtained via qPAINT (red) vs. lbFCS (blue) at *c* = *5* nM as in **Figure 4**b. The black dashed line displays a line through the origin of slope one as expected for ideal counting results (i.e. $N_{out} = N_{in}$). The first qPAINT data point at *N* = 48 deviating from the ideal behavior is indicated by a black arrow. Bottom: histogram showing the number of unique dark times per intensity vs. time trace for the *N* = 48 qPAINT data point. The dashed red line indicates the minimum of three unique dark times per intensity trace required for the fit described in **Supplementary Figure 7**. In case a trace exhibited less than three unique dark times, we assigned the mean dark time obtained over all fits to the cluster. Clusters, i.e. traces featuring no dark time at all were discarded from further analysis. (b) Top: same as in (a), but for *c* = 10 nM. Bottom: the majority of clusters in the data set indicated by the black arrow at *N* = 30 exhibit less than the required three unique dark times. (c) Same as in (a-b), but for *c* = 20 nM. Histogram of unique dark times displayed for the data point at *N* = 18.

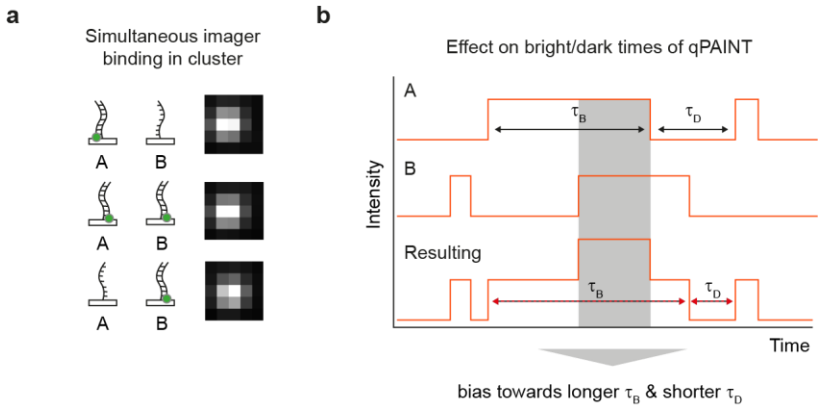

Supplementary Figure 10. Simultaneous binding in dense clusters limits qPAINT. (a) Schematic of the case of simultaneous binding of imagers to two docking strands A and B in close proximity. The diffraction limited images indicate an increase in fluorescence intensity when an imager is bound to both docking strands compared to when only a single imager is bound. (b) Individual intensity vs. time traces for DS A and B. The duration of simultaneous binding is shaded in grey. The resulting intensity vs. time trace (bottom) extracted from the localization cluster of the two DSs exhibits an extended bright event and shortened dark event (black-red dashed double arrows) when analyzed according to qPAINT (see **Supplementary Figure 7**). To avoid simultaneous binding events limiting this approach the imager concentration has to be adjusted accordingly to the expected target density.

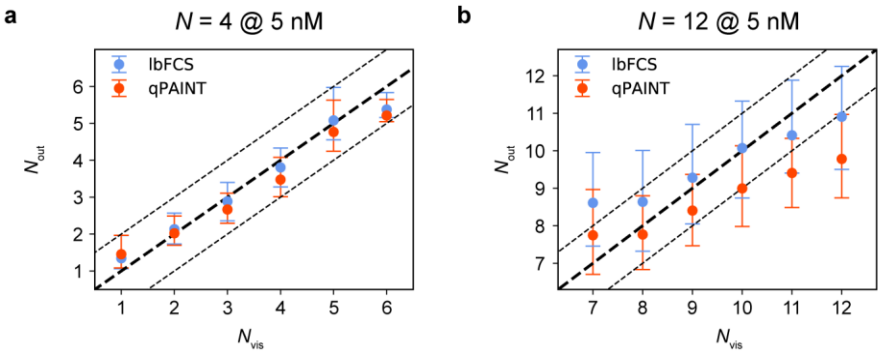

Supplementary Figure 11. N_{out} vs. N_{vis} comparison per integer from visual counting results. (a) lbFCS/qPAINT counting results for the N = 4 data set at c = 5 nM compared to visual counting results. The bold black line indicates the line through the origin of slope one as expected for ideal counting (i.e. N_{out} = N_{vis}). The light black dashed lines indicate a counting error of $\pm$ 1. This implies that for each N_{vis} more than 50 % of all clusters fulfill the criterion abs(N_{out} – N_{vis}) < 1. (b) Same as in (a) but for the N = 12 data set at c = 5 nM. Error bars correspond to interquartile range.

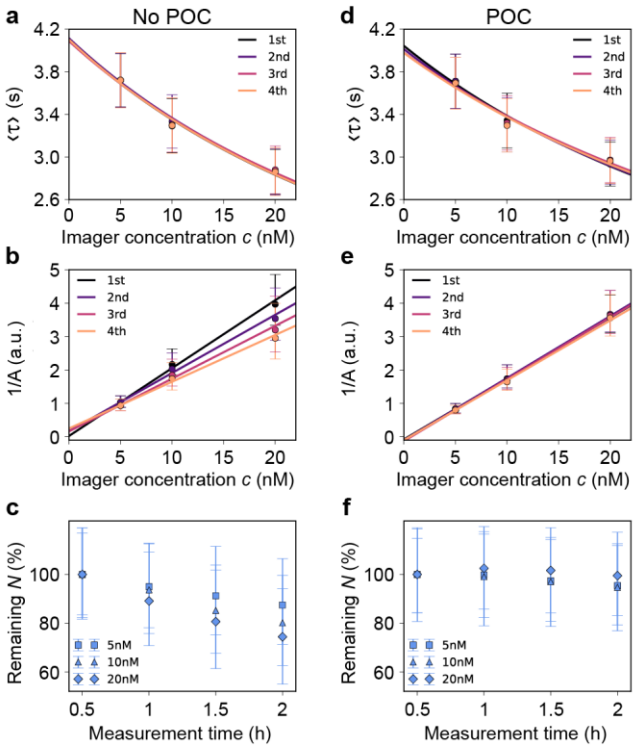

Supplementary Figure 12. Depletion of docking strands for DNA-PAINT imaging at low laser power. (a) Three-point concentration series for DNA origami samples (N = 12) each measured for 2 h (4 × longer than standard lbFCS measurement time). The data sets were temporally divided into 4 segments and each analyzed via lbFCS. The four respective overlapping ⟨τ⟩ vs. c fits yield that neither of the global parameters k_{on}, k_{off} and c changed over the acquisition time. (b) In contrast, the four 1/A vs. c fits clearly change over time as a result of DS depletion occurring even at low laser power. (c) DS depletion rate normalized to the lbFCS counting results from the first segment. (d) Repeat of the same concentration series as in (a) with POC + Trolox added to the imaging solution also indicating constant global parameters over time. (e) In contrast to (b) with POC + Trolox 1/A does also not change over time. (f) Negligible depletion rate of DS for POC + Trolox. Error bars in (c) and (f) correspond to interquartile range.

Supplementary Table 1 | Total number of analyzed clusters for lbFCS/qPAINT counting

N	*c* (nM)	No. of automatically detected clusters	No. of clusters after filtering	No. of clusters after removal of $N_{vis} = 0$	No. of clusters for lbFCS analysis	No. of clusters for qPAINT analysis	Reference
4	5	28,166	12,815	10,963	10,963	10,963	**Figure 4d** (top)
4	10	18,824	6,343	5,245	5,245	5,245	**Figure 4d** (middle)
4	20	24,775	7,399	6,090	6,090	6,090	**Figure 4d** (bottom)
12	5	3,825	1,782	1,781	1,781	1,781	**Figure 4e** (top)
12	10	4,288	1,779	1,778	1,778	1,777	**Figure 4e** (middle)
12	20	3,662	1,200	1,200	1,200	1,171	**Figure 4e** (bottom)
48	5	9,743	3,829	n.a.	3,829	3,822	**Figure 4f** (top)
48	10	3,899	1,653	n.a.	1,653	1,496	**Figure 4f** (middle)
48	20	9,949	1,584	n.a.	1,584	419	**Figure 4f** (bottom)

Supplementary Table 2 | Used DNA-PAINT sequences

Shortname (docking strand length)	Docking strand sequence	Imager sequence	Experiment
PS6 (8 nt)	TT TCCTCCTC	GAGGAGGA-Cy3b	All experiments

Supplementary Table 3 | Parameters for analysis steps

Module	Parameters
localize	Net gradient = 400 Quantum efficiency = 0.82 (from Camera Specs) Sensitivity = 0.53 (from Camera Specs) Box size = 5 pixel Background = 70
render : undrift	No of segments for RCC drift correction: 500
autopick	Oversampling = 5 Net gradient = 300
render : picked	Pick diameter = 2 pixel
pickprops	Ignore = 1 (for qPAINT analysis, see **Supplementary Figure 7**)
filter	n.a.

Supplementary references

1. Schnitzbauer, J., Strauss, M. T., Schlichthaerle, T., Schueder, F. & Jungmann, R. Super-resolution microscopy with DNA-PAINT. *Nat. Protoc.* **12**, 1198 (2017).
2. Strauss, M. T., Schueder, F., Haas, D., Nickels, P. C. & Jungmann, R. Quantifying absolute addressability in DNA origami with molecular resolution. *Nat. Commun.* **9**, 1600 (2018).
3. Stehr, F., Stein, J., Schueder, F., Schwille, P. & Jungmann, R. Flat-top TIRF illumination boosts DNA-PAINT imaging and quantification. *Nat. Commun.* **10**, 1268 (2019).
4. Edelstein, A. D. *et al.* Advanced methods of microscope control using μManager software. *J. Biol. Methods; Vol 1, No 2* (2014).
5. Mücksch, J. *et al.* Quantifying Reversible Surface Binding via Surface-Integrated Fluorescence Correlation Spectroscopy. *Nano Lett.* **18**, 3185–3192 (2018).
6. Jungmann, R. *et al.* Single-Molecule Kinetics and Super-Resolution Microscopy by Fluorescence Imaging of Transient Binding on DNA Origami. *Nano Lett.* **10**, 4756–4761 (2010).
7. Jungmann, R. *et al.* Quantitative super-resolution imaging with qPAINT. *Nat. Methods* **13**, 439 (2016).